

An Adaptive Multigrid Method for Modeling Photon Transport through Biological Tissues in Bioluminescence Tomography

Kai Liu, Jie Tian*, *Senior member, IEEE*, Pu Wang, Dan Liu, Yujie Lv, Min Xu and Chenghu Qin

Abstract—In this paper, we develop an Adaptive Multigrid method (AMGM) to model photon transport through biological tissues in bioluminescence tomography. In our method, the smoothing operation on fine levels and residual correction on coarse levels in V-Cycle offer fast convergence rate for this forward problem. Using a heterogeneous phantom, the methodology is validated by Monte Carlo simulations, and the computation speed is much higher than conventional smoothing iteration methods on a single grid. In actual biomedical imaging applications, especially when there are many sources in small animal body, AMGM is potential to accurately simulate the forward problem at very low computation cost.

I. INTRODUCTION

Molecular tomography such as bioluminescence tomography (BLT) can be used to localize and quantify several important bioluminescent enzymes to elucidate molecular and cellular signatures or pathways in intact biological tissues. As an important part of the study, accurate modeling of photon transport through biological media has been received increased attention in recent years [1]. Unlike X-rays used in medical CT, photons undergo multiple absorption and scattering before leaving the tissues. A widely accepted model for this process is the radiative transfer equation (RTE) [2], which is a complex integro-differential equation. The diffusion approximation (DA) is basically a first order approximation of RTE. Owing to low tissue absorption in the near-infrared (NIR) spectral window, light penetration through considerable depths of tissue is possible. Hence the DA can model photon transport through tissues effectively in this spectral range.

In recent years, various DA-based methods have been presented to model diffuse photon transport in optical imaging. Analytic solutions to DA in some simplified cases [3], [4] have been explored. Their analytical results are in good agreement with the Monte Carlo simulations. In order to apply the analytical approximation for complex

boundaries and volumes, Ripollet *et al.* [5] presented the Kirchhoff approximation. The utilization of numerical methods is generally preferred for complex boundaries, and some numerical methods have been explored. Arridge *et al.* [6] introduced a finite element method (FEM) based on DA for deriving photon density inside an object, and photon flux at its boundary. It modeled the boundary flux density as a function of time resulting from δ -function input to a two-dimensional circle on a single grid. Lv *et al.* [7] applied the adaptive FEM framework into the forward problem of BLT, to achieve better spatial resolution for the source distribution and strength reconstruction in BLT.

More recently, in order to increase computational efficiency, multigrid algorithms have been used for medical imaging applications such as in electrical impedance tomography (EIT) and diffuse optical tomography (DOT). Borcea [8] used a nonlinear multigrid approach to EIT based on a direct nonlinear formulation in nonlinear multigrid partial differential equation solvers. Seungseok *et al.* [9] formulated the multigrid inversion directly in an optimization framework. It has been shown that this algorithm can highly reduce computation cost when the inversion problem is solved to achieve a high-quality reconstruction.

In this study, an Adaptive Multigrid method (AMGM) framework is presented to model photon transport within the biological tissues based on DA in BLT. FEM which is chosen to build our AMGM framework, will be introduced at the beginning. Nodal basis functions for sources are emphasized since they are linear (C^0 continuous), while the element basis functions are not continuous. Then, our adaptive multigrid methods are presented elaborately. Finally, we compare the approximation using AMGM with the simulation results from MOSE based Monte Carlo method, and demonstrate the validity of AMGM. Moreover, compared with smoothing iteration methods on a single grid, our AMGM provides a fast algorithm for modeling photon transport in biological tissues.

II. DIFFUSION EQUATION AND ITS FINITE ELEMENT FORMULATION

In bioluminescence imaging, the photon transport process can be modeled by the steady-state, time-independent diffusion equation. Using the Galerkin method, the equivalent variation formulation of diffusion equation in which $\Phi(x) \in$

This work is supported by the Project for the National Basic Research Program of China (973) under Grant No.2006CB705700, Changjiang Scholars and Innovative Research Team in University (PCSIRT) under Grant No.IRT0645, CAS Hundred Talents Program, CAS scientific research equipment develop program (YZ0642,YZ200766), 863 program under Grant No. 2006AA04Z216, the Joint Research Fund for Overseas Chinese Young Scholars under Grant No.30528027, the National Natural Science Foundation of China under Grant No. 30672690, 30600151, 30500131, 60532050, Beijing Natural Science Fund under Grant No. 4071003.

Kai Liu, Jie Tian, Dan Liu, Yujie Lv, Min Xu and Chenghu Qin are with Medical Image Processing Group, Institute of Automation, Chinese Academy of Sciences, P. O. Box 2728, Beijing 100190, China, e-mail: tian@ieee.org

Pu Wang is with Department of Electronic Information&Control Engineering, Beijing University of Technology Beijing, 100124, China.

$H_0^1(\Phi)$ can be satisfied is described as[10]:

$$\left\{ \begin{array}{l} \int_{\Omega} (D(x)\nabla\Phi(x)\nabla\Psi(x) + \mu_a(x)\Phi(x)\Psi(x))dx + \\ \int_{\partial\Omega} \frac{\Phi(x)\Psi(x)}{2A(x;n,n')}dx = \int_{\Omega} S(x)\Psi(x)dx \quad (\forall\Psi(x) \in H_0^1(\Omega)) \end{array} \right. \quad (1)$$

where Ω and $\partial\Omega$ denote the domain of interest and the boundary of the domain respectively, $\Phi(x)$ the flux density [W/mm^2] at location x , $\Psi(x)$ the test functions, $S(x)$ the source energy density [W/mm^3], μ_a the absorption coefficient [mm^{-1}], $D(x) = 1/(3(\mu_a + (1-g)\mu_s))$ the optical diffusion coefficient [mm], μ_s the scattering coefficient [mm^{-1}], g the anisotropy parameter. $A(x;n,n')$ is a function that represents refractive index mismatch between tissue and the surrounding medium.

To solve the Eq. 1 on a computer, the infinite dimensional function space Ω should be substituted by a finite dimensional approximation Ω^h consisting of N_p vertex nodes and N_e elements (e.g. tetrahedral), denoted as Ω^l ($l = 1, 2, \dots, N_e$), such that $\Omega^h = \bigcup_{l=1}^{N_e} \Omega^l$. Hence Ω is partitioned into continuous and piecewise polynomial functions [10]:

$$\Phi(x) \approx \Phi^h(x) = \sum_{k=1}^{N_p} \phi_k \varphi_k(x) \text{ when } x \in \Omega^h(x) \quad (2)$$

where ϕ_k is the value of $\Omega(x)$ on the k -th node, and $\varphi_k(x)$ the nodal basis function within the elements Ω^l . Similarly, the source function $S(x)$ is approximated as [10]:

$$S(x) \approx S^h(x) = \sum_{k=1}^{N_p} s_k \varphi_k(x) \text{ when } x \in \Omega^h(x) \quad (3)$$

s_k is the value of $S(x)$ on the k -th node. We choose the same nodal basis functions as $\Phi(x)$, which are C^0 and can be more accurate than the element basis functions [7].

Substituting Eqs. 2 and 3 into Eq. 1, and using the nodal basis functions $\varphi_k(x)$ as the basis functions, we obtain the matrix equation as follows [10]:

$$(K + C + B)\Phi = M\Phi = FS = b \quad (4)$$

III. ADAPTIVE MULTIGRID METHOD

A. Multigrid Algorithm

According to the theory of finite element methods [11], the condition number of the stiff matrix M is $O(h^{-2})$, in which h denotes the dimension of elements. As the grid is refined, the condition number becomes larger and even approaches infinity. Therefore, when only the classical iteration methods such as Jacobi and Conjugate Gradient methods are applied to resolve Eq. 4 on a single grid (SG), the convergence rate is very slow.

However, the multigrid methods present fast convergence rate, which combines two complementary schemes. Firstly, applying iterative methods hereinbefore, the high-frequency components of the error on a single level are reduced. For this reason these methods are called smoothers. Secondly, low-frequency error components are effectively reduced by

a coarse-grid correction procedure. As smooth error components are left by the smoothing iterations, it is possible that its solution is an approximation to the coarser system. After this coarser problem is solved, its solution is interpolated back to fine grids to correct the approximation on fine grids for its low-frequency errors. In practice, this interpolation procedure may cause high-frequency errors on fine grids. Therefore it is better to apply post-smoothing sweeps after correction on coarse grids [12]. The Multigrid Algorithm for solving Eq. 4 is summarized as the following scheme[12]:

1. If $k = 0$, solve $M_k\Phi_k = b_k$ directly, else pre-smoothing on this fine grid: $\Phi_k^l := \text{Smooth}(\Phi_k^{l-1}, b_k), l = 1, \dots, \nu_1$;
2. Computation of the residual: $r_k = b_k - M_k\Phi_k^{\nu_1}$;
3. Restriction of the residual: $r_{k-1} = I_{k-1}^{k-1}r_k$;
4. Call the MG scheme to solve $M_{k-1}\Phi_{k-1} = b_{k-1}$;
5. Coarse-grid correction: $\Phi_k^{\nu_1} := \Phi_k^{\nu_1} + I_{k-1}^k\Phi_{k-1}$;
6. Post-smoothing on fine grid: $\Phi_k^l := \text{Smooth}(\Phi_k^{l-1}, b_k), l = \nu_1 + 1, \dots, \nu_1 + \nu_2$ then if $\|b_k - M_k\Phi_k^{\nu_1+\nu_2}\|_2/\|b_k\|_2 > \text{threshold}$, then skip to step 1, else stop.

where k denotes the grid level, and I_{k-1}^{k-1} and I_{k-1}^k represent restriction and prolongation operator. $\text{Smooth}(\Phi_k^{l-1}, b_k)$ is the smooth iteration. *Threshold* is a parameter governing the computation accuracy. In modifying the value of *threshold*, the approximations of different accuracy may be obtained. The algorithm is represented as V-Cycle (Fig.1).

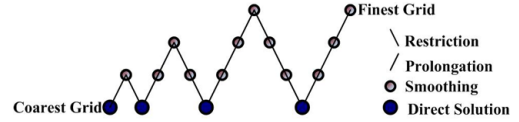


Fig. 1. V-cycle for the full multigrid algorithm.

B. Adaptive method in full multigrid algorithm

In dealing with Eq.4, it is important to start the iterative procedure with a suitable initial approximation. We apply the nested iteration technique to naturally get the first guess cheaply. The whole process starts from the coarsest level in which the discretized problem $M_k\Phi_k = b_k$ is easily resolved. Therefore this solution could be interpolated to the next finer level as the initial guess on the new grid for the pre-smoothing $M_{k+1}\Phi_{k+1} = b_{k+1}$. The algorithm combining the multigrid method with nested iteration is called full multigrid algorithm [12], which is illustrated by full V-cycle in Fig.1.

In fact, all the fine grids used in the full multigrid algorithm are adaptively refined from an initial coarse grid. Three steps are gone through in sequence. Firstly, estimate the error on each element according to a posteriori error estimator based on the solution on coarse levels. Quadratic basis functions (C^1 continuous), which are comprised of both the nodes on vertices and the midpoints on the edges as the node bases are used for estimating the errors. Secondly, tag the elements of the coarse grids for refinement where the local errors are large. Finally, according to the tags, grids are adaptively refined.

In dealing with refinement, two sets of basis functions are employed for finite element space Ω^k on each level: the

nodal basis $\varphi_l^k(x), l = 1, \dots, n_k$ and the hierarchical basis $\hat{\varphi}_l^k(x), l = 1, \dots, n_k$. The nodal basis has been explained in section 2, and the hierarchical basis of Ω^k consists of the hierarchical basis functions $\hat{\varphi}_l^k(x), l = 1, \dots, n_{k-1}$ of the Ω^{k-1} and the nodal basis functions $\hat{\varphi}_l^k(x) := \varphi_l^k(x), l = n_{k-1} + 1, \dots, n_k$ on Ω^k [14]. The spanned space of the nodal basis functions on Ω^k is denoted by v^k . It is newly generated in the refinement from level $k - 1$ to k .

Hence in the hierarchical basis representation, the Ω^k is partitioned into $\Omega^k = \Omega^{k-1} \oplus v^k$. Naturally, the hierarchical basis of Ω^k induces a natural partitioning of the space:

$$\Omega^k = v^1 \oplus v^2 \oplus \dots \oplus v^k \quad (5)$$

At the end of refinement, there are more nodes around singularities to equilibrate error on each element, with the nodes in the smooth regions unchanged [13].

IV. NUMERICAL EXPERIMENTS

In our bioluminescence imaging experiments, we choose a heterogeneous mouse phantom that contains organs including muscle, lungs, heart, liver, and bone, and it has a height of $30mm$ and radius of $10mm$, as shown in Figure IV. Four sphere bioluminescent sources with $1.0mm$ radius and $238pW/mm^3$ power density are embedded in the phantom, with the location of $(13,-4,-4)$, $(17,-4,-4)$, $(13,-4, 4)$, $(17,-4, 4)$, as shown in Fig.2. Four simulation experiments have been done, with S_1 in the first experiment, S_1 and S_2 in second, S_1, S_2 and S_3 in third, and all in fourth. The optical properties of the heterogeneous phantom are listed in Table I. The refractive index for all regions in the phantom is 1.37.

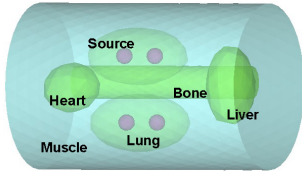


Fig. 2. A heterogeneous phantom with regions geometrically similar to muscle, lungs, heart, liver, and bone, respectively, and four sphere sources located in two lungs.

A. Simulating experiment results using Monte Carlo method

We use MOSE (A mouse optical simulation environment) based on Monte Carlo method to simulate biomedical experiments using the mouse phantom, which is the gold standard for this forward problem [15]. The grids used in MOSE are structured by surface triangles for each region. In our experiments the phantom is discretized into 39570 triangular

TABLE I
OPTICAL PARAMETERS FOR EACH REGION IN THE PHANTOM

Region	$\mu_a [mm^{-1}]$	$\mu_s [mm^{-1}]$	g
Muscle	0.01	4.0	0.90
Heart	0.2	16.0	0.85
Lung	0.35	23.0	0.94
Liver	0.035	6.0	0.90
Bone	0.002	20.9	0.90

TABLE II
GRID PARAMETERS BEFORE AND AFTER SIMULATIONS

Number of sources	1	2	3	4
Coarest Nodes	2157	2252	2757	2868
Coarest Elements	10458	10932	13049	13690
Finest Nodes	35201	80803	115056	128443
Finest Elements	204030	472339	672194	749866
Discretization Error(%)	0.352	0.398	0.391	0.440

elements with the maximum dimension of $0.8mm$. A total of 158536 virtual detectors are allocated on the surface of phantom to record exiting flux density. Each source is assumed to obey uniform distribution and sampled to 10^6 photon packets.

B. Modeling photon transport using Adaptive Multigrid Method

In each AMGM simulation, the number of nodes and tetrahedrons for the discretized phantom on the coarsest level are listed in Table II, and the maximum dimension for all elements is $2.0mm$. At the beginning, the problem is directly solved by triangular factorization on the coarsest level, which is employed as initial approximation. In the V-Cycle, we choose symmetric Gauss-Seidel method as the preconditioner for pre-smoothing and post-smoothing.

In order to reach high accuracy, the initial grids are highly refined during the full multigrid cycle. The nodes and elements for each grid on finest level and the discretization error for 4 experiments are shown in Table II. Fig.3 shows the matching curves for the MOSE results, and AMGM simulations along detection circle at $x = 13mm$ on the surface. The relative errors between AMGM and MOSE for the 4 experiments are 0.717%, 0.675%, 0.701%, 0.709%, respectively. It can be seen the AMGM is well consistent with the results from Monte Carlo simulation, and its accuracy is almost the same as SG.

Finally, to demonstrate the efficiency of AMGM, we also compare our algorithm with SG, in which only conventional smoothing is used and V-Cycle not. Conjugate Gradient method is selected as a smoother for SG. In our experiment, the SG are iterated on the finest grid of AMGM listed in Table II and its exiting flux density along detection circle is

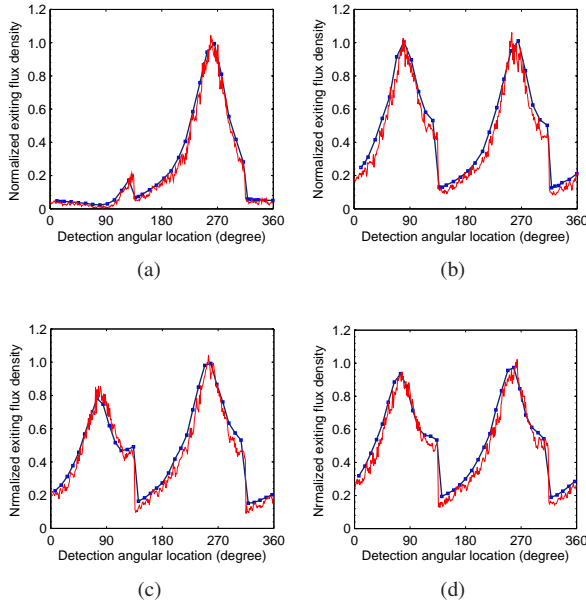


Fig. 3. Comparing exiting flux density of AMGM, SG and MOSE along detection circle at $x=13\text{mm}$. The blue square represents the AMGM data, the blue solid SG, and the red solid line is the MOSE data. (a) Experiment 1 with one source; (b) experiment 2 with two sources; (c) experiment 3 with three sources; and (d) experiment 4 with four sources.

also painted in Fig.3. It is seen that the efficiency of AMGM is much higher than SG using Conjugate Gradient iterations as shown in Fig.4. All the simulations are done on a Intel Core 2 Duo 1.86GHz PC with 2GB RAM.

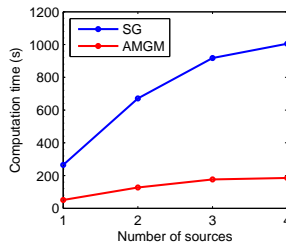


Fig. 4. The computation time for AMGM and SG on condition of same discretization error as listed in Table II.

V. DISCUSSION AND CONCLUSIONS

In this paper, we represent an adaptive multigrid method (AMGM) to model photon transport through biological tissues in BLT. Actually, AMGM can be applied to the forward problem of other optical imaging applications, *e.g.* fluorescence molecular tomography (FMT).

This work demonstrates the merits of AMGM. In the V-Cycle, the smoothing process on fine grids and the correction

on coarse grids reduce high and low frequency residual respectively. Comparing Monte Carlo simulations, AMGM matches well with the former, so it is valid for the forward problem. The other promising feature is its fast computation speed. For low frequency residual correction is operated on the coarse levels, along with adaptive method, the cost of computation is extremely reduced. Comparing run time between AMGM and SG in Figure 4, AMGM uses much less time than its counterpart. Moreover, with number of sources increased, the cost of AMGM rises slower than SG. Actually in BLT or FMT experiments, there are many fluorescence or bioluminescence sources distributing among different organs. Hence, our AMGM is competent for actual biomedical experiments to highly reduce run time.

REFERENCES

- [1] A. P. Gibson, J. C. Hebden, and S. R. Arridge, "Recent advances in diffuse optical imaging," *Phys. Med. Biol.*, vol.50, no.4, pp.R1-R43, 2005.
- [2] L. V. Wang, H. Wu, *Biomedical Optics*, Wiley-Interscience, New York, USA, 2007.
- [3] S. R. Arridge, M. Cope, and D. T. Delpy, "The theoretical basis for the determination of optical pathlengths in tissue: temporal and frequency analysis," *Phys. Med. Biol.*, vol. 37, no. 7, pp. 1531-1560, 1992.
- [4] W. Cong, L. V. Wang, and G. Wang, "Formulation of photon diffusion from spherical bioluminescent sources in an infinite homogeneous medium," *BioMedical Engineering OnLine*, vol. 3, no. 7, 2004. <http://www.biomedical-engineering-online.com/content/3/1/12>
- [5] J. Ripoll, D. Yessayan, G. Zacharakis, and V. Ntziachristos, "Experimental determination of photon propagation in highly absorbing and scattering media," *J. Opt. Soc. Am. A*, vol.22, no.3, pp.546-550, 2005.
- [6] S. R. Arridge, M. Schweiger, M. Hiraoka, and D. T. Delpy, "A finite element approach for modeling photon transport in tissue," *Medical Physics*, vol. 20, no. 2, pp.299-309, 1993.
- [7] Y. Lv, J. Tian, H. Li, J. Luo, W. Cong, G. Wang and D. Kumar, "Modeling the forward problem based on the adaptive FEMs framework in bioluminescence tomography," *Proceedings of the SPIE on Optics & Photonics*, San Diego, California USA, vol. 6318, pp. 63180I, Sep. 7, 2006.
- [8] L. Borcea, "Nonlinear multigrid for imaging electrical conductivity and permittivity at low frequency," *Inverse Problems*, vol. 17, no. 2, pp. 329-359, 2001.
- [9] Oh, Seungseok, A.B. Milstein, C.A. Bouman, K.J. Webb, "A general framework for nonlinear multigrid inversion," *IEEE Transactions on image Processing*, vol. 14, no. 1, pp. 125-140, 2005.
- [10] W. Cong, G. Wang, D. Kumar, Y. Liu, M. Jiang, L. Wang, E. Hoffman, G. McLennan, P. McCray, J. Zabner, and A. Cong, "Practical Reconstruction Method for Bioluminescence Tomography," *Opt. Express*, vol. 13, no. 18, pp. 6756-6771, 2005.
- [11] S. C. Brenner, L. C. Scott, *The Mathematical Theory of Finite Element Methods*, Springer-Verlag, New York, USA, 1994.
- [12] W. Hackbusch, *Multi-Grid Methods and Applications*, Springer-Verlag, Heidelberg, Germany, 1985.
- [13] P. Bastian, C. Wieners, "Multigrid Methods on Adaptively Refined Grids," *Computing in Science & Eng.*, vol. 8, no. 6, pp. 12-22, 2006.
- [14] R. E. Bank, T. F. Dupont, and H. Yserentant, "The hierarchical basis multigrid method," *Numer. Math.*, vol. 52, no. 4, pp. 427-458, 1988.
- [15] H. Li, J. Tian, *et al.*, "A mouse optical simulation environment (MOSE) to investigate bioluminescent phenomena in the living mouse with the Monte Carlo Method," *Acad. Radiol.*, vol. 11, no. 9, pp. 1029-1038, 2004.